ARL-TR-10050 ● JAN 2025

Highly Efficient CO_2 Conversion to Energy-Dense Fuels with Hybrid Electrochemical Membrane Electrode Assembly (MEA) Technologies

by David R. Baker, Vijay Parameshwaran, Jonathan Boltersdorf, and Rongzhong Jiang

NOTICES

Disclaimers

The findings in this report are not to be construed as an official Department of the Army position unless so designated by other authorized documents.

Citation of manufacturer's or trade names does not constitute an official endorsement or approval of the use thereof.

Destroy this report when it is no longer needed. Do not return it to the originator.

ARL-TR-10050 ● JAN 2025

Highly Efficient CO_2 Conversion to Energy-Dense Fuels with Hybrid Electrochemical Membrane Electrode Assembly (MEA) Technologies

David R. Baker, Vijay Parameshwaran, Jonathan Boltersdorf, and Rongzhong Jiang
DEVCOM Army Research Laboratory

REPORT DOCUMENTATION PAGE

1. REPORT DATE	2. REPORT TYPE	3. DATES COVERED	
		START DATE	END DATE
January 2025	Technical Report	2 October 2023	1 November 2024

4. TITLE AND SUBTITLE
Highly Efficient CO_2 Conversion to Energy-Dense Fuels with Hybrid Electrochemical Membrane Electrode Assembly (MEA) Technologies

5a. CONTRACT NUMBER	5b. GRANT NUMBER	5c. PROGRAM ELEMENT NUMBER
5d. PROJECT NUMBER	**5e. TASK NUMBER**	**5f. WORK UNIT NUMBER**

6. AUTHOR(S)
David R. Baker, Vijay Parameshwaran, Jonathan Boltersdorf, and Rongzhong Jiang

7. PERFORMING ORGANIZATION NAME(S) AND ADDRESS(ES)	8. PERFORMING ORGANIZATION REPORT NUMBER
DEVCOM Army Research Laboratory ATTN: FCDD-RLA-GC Adelphi, MD 20783-1138	ARL-TR-10050

9. SPONSORING/MONITORING AGENCY NAME(S) AND ADDRESS(ES)	10. SPONSOR/MONITOR'S ACRONYM(S)	11. SPONSOR/MONITOR'S REPORT NUMBER(S)
Office of Naval Research		

12. DISTRIBUTION/AVAILABILITY STATEMENT
DISTRIBUTION STATEMENT A. Approved for public release: distribution unlimited.

13. SUPPLEMENTARY NOTES
ORCIDs: David R. Baker: 0000-0002-9930-5183; Vijay Parameshwaran: 0009-0004-0288-9170; Jonathan Boltersdorf: 0000-0002-1105-0711; Rongzhong Jiang: 0000-0002-5233-3312

14. ABSTRACT
This report demonstrates highly efficient carbon dioxide (CO_2) conversion into energy-dense fuels using hybrid electrochemical technologies, including electrochemical plating (ECP) of copper (Cu)-thin film catalysts on gas diffusion layers (GDLs), electrode surface optimization by corrosion/reduction treatment, and advanced zero-gap reactor design with alkaline membrane electrode assemblies (MEAs). Cu/GDLs are used as cathodes to assemble a zero-gap electrochemical reactor with an alkaline polymer electrolyte membrane and a catalyst-coated anode. The reactors show high product selectivity and electrochemical activity for converting CO_2 to ethylene (C_2H_4). At low operating temperatures (20–30 °C), and 3.0 V cell voltage, the Faradaic efficiency reaches up to 83% for C_2H_4 generation and nearly 100% for total CO_2 reduction reaction (CO2RR). At 60 °C and 3.0 V cell voltage, the electrochemical current density reaches 131 mA/cm^2 for C_2H_4 generation and nearly 200 mA/cm^2 for the total CO2RR. Gaseous fuels generated from the reactor are analyzed with gas chromatography. The synthesis ratio of C_2H_4 to carbon monoxide is highly dependent on ECP conditions for preparation of the Cu/GDL cathode electrode, which gives a form of control over the C2 to C1 product ratio of the CO2RR.

15. SUBJECT TERMS
Energy Sciences, carbon dioxide, alternative fuels, electrochemistry, ethylene, membrane, electrodeposition, copper, plating

16. SECURITY CLASSIFICATION OF:			17. LIMITATION OF ABSTRACT	18. NUMBER OF PAGES
a. REPORT	b. ABSTRACT	C. THIS PAGE		
UNCLASSIFIED	UNCLASSIFIED	UNCLASSIFIED	UU	33

19a. NAME OF RESPONSIBLE PERSON	19b. PHONE NUMBER *(Include area code)*
David R. Baker	(301) 394-2249

STANDARD FORM 298 (REV. 5/2020)
Prescribed by ANSI Std. Z39.18

Contents

List of Figures

List of Tables

Acknowledgments

We are grateful to the Office of Naval Research for funding under the Blue Carbon-Direct Carbon Capture program.

1. Introduction

The electrochemical method to convert carbon dioxide (CO_2) to fuel is the reverse chemical process of burning fossil fuels and provides a controlled means to generate fuel from atmospheric, seawater, or combustion CO_2 resources.[1–5] Ideal CO_2 reduction reaction (CO2RR) catalysts have been sought with properties of high catalytic activity, long-term stability, and good selectivity, which are largely dependent on unique nanomaterial development at electrode surfaces.[2,3,5–9] In addition, highly efficient electrochemical reactor designs are necessary to convert CO_2 to usable fuels at production rates sufficient for the industrial scale, or at the pace of Army operations.[4,10–18] In the present research, we constructed an electrochemical system based on a zero-gap alkaline membrane electrode assembly (MEA) reactor design and successfully carried out catalyst research on CO2RR. There are still many challenges remaining. In the electrochemical CO2RR process, a large amount of H_2 byproduct is generated because of the hydrogen evolution reaction (HER), which results in low CO2RR Faradaic efficiency (F_{eff}). Furthermore, a major carbon-based product of CO2RR is carbon monoxide (CO), a poisonous gas with low-energy pathway that involves only a two-electron reduction reaction of CO_2. In the process of CO2RR, we also obtained a small amount of ethylene (C_2H_4) by 12-electron reduction of CO_2. If we can increase the yield of C_2H_4, we will obtain a greener chemical fuel with much higher energy density ($\Delta H_c^\circ = -1441$ kJ/mol). For pursuing even higher C_2 product selectivity and catalytic current density for CO2RR, we explored a new technology of nanostructured catalyst synthesis at the electrode surface. Copper (Cu) electrochemical plating (ECP) technology is widely used in the electronics and semiconductor industry for plating smooth Cu layers on electric circuit boards.[19] However, directly depositing Cu nanocrystals on polytetrafluoroethylene (PTFE)-containing porous gas diffusion layers (GDLs) for catalysts has not been reported yet. The advantage of Cu-plating at the electrode surface is that the Cu/GDL can be directly used as an electrode for assembling alkaline MEA reactors. The catalyst morphology, particle size, composition, and catalytic properties can be tailored by controlling current, voltage, and electrolyte composition. In addition, we explored methods of optimizing catalyst morphology at the cathode surface by corrosion/reduction treatment (CRT). The three approaches of ECP, CRT, and zero-gap reactors form hybrid electrochemical technologies to achieve the highly efficient electrochemical conversion of CO_2 to an energy-dense fuel.

2. Equations

The F_{eff} of CO2RR is calculated with following equation,[18]

$$F_{eff} = \frac{xVPnF}{IRT} \times 100\% \quad (1)$$

If we do not compress the cell, the gas pressure (P) in the MEA reactor should be at one atmosphere. For ease of use, we converted Equation 1 to a clear equation for actual calculations of the data from the reactor of CO2RR and the gas chromatograph (GC),

$$F_{eff} = x \cdot \left(\frac{\dot{V}}{60} \cdot \frac{1}{1000}\right) \cdot \frac{P}{0.082(t+273)} \cdot n \cdot F \cdot \frac{1}{I} \cdot 100\% \quad (2)$$

Here, x is the fraction of a gas product obtained from the GC; $\dot{V}$ (sccm, or mL/mim) is the flow rate from the cathode of the reactor; P (atm) is gas pressure; R is gas constant (R = 0.082 L atm·mol^{-1}·K^{-1}), T is the temperature in Kelvin (K), t is common temperature (Celsius), n is the number of electrons transferred in electrochemical reaction; F is the Faraday constant (96,485 s·A·mol^{-1}), and I is current (A) from the electrochemical cell.

The electrochemical reactions and formal potentials at the cathode are as follows:[1]

$$CO_2 + 2H^+ + 2e^- \rightarrow CO(g) + H_2O \quad (E^0 = -0.1\ V) \quad (3)$$

$$CO_2 + 2H^+ + 2e^- \rightarrow HCOOH(eq) \quad (E^0 = -0.12\ V) \quad (4)$$

$$2H^+ + 2e^- \rightarrow H_2 \quad (E^0 = 0\ V) \quad (5)$$

$$CO_2 + 8H^+ + 8e^- \rightarrow CH_4(g) + 2H_2O \quad (E^0 = 0.17\ V) \quad (6)$$

$$2CO_2 + 12H^+ + 12e^- \rightarrow C_2H_4(g) + 4H_2O \quad (E^0 = 0.08\ V) \quad (7)$$

The electrochemical reactions at the anode are as follows:

$$2H_2O \rightarrow O_2 + 4H^+ + 4e^- \quad (E^0 = 1.23\ V) \quad (8)$$

$$HCOOH(eq) \rightarrow CO_2 + 2H^+ + 2e^- \quad (E^0 = -0.12\ V) \quad (9)$$

The energy efficiency (E_{eff}) of CO2RR is calculated as follows:

$$E_{eff} = F_{eff}(E^0{}_a - E^0{}_c)/E_{cell} \quad (10)$$

Here, $E^0{}_a$, $E^0{}_c$, and E_{cell} (in volts) are anode standard potential, cathode standard potential, and total cell voltage obtained from experiment, respectively.

We emphasize that F_{eff} is a description of catalytic selectivity. The total F_{eff} of all products would be 100%, including byproducts. The total measured F_{eff} from the product gas stream will be less than 100% owing to the product $HCOO^-$ at the cathode that crosses over to the anode and is oxidized to form CO_2 again (see Equation 9). The E_{eff} is a description of the sum of catalytic selectivity and activity. The cell catalytic performance of CO2RR can be described with the two factors of F_{eff} and E_{eff}. The third important factor is catalytic current density (j_x) of CO2RR, which describes the amount of product produced per unit electrode area and per unit time. Finally, the fourth important factor is catalytic stability, which can be obtained by long-term operation of the CO2RR reactor. These four factors quantitatively described the cell performance for electrochemically converting CO_2 to fuels.

The gas products from the CO2RR reactor were analyzed with a GC, which contained a flame ionization detector (FID). The FID detector in the GC included a methanizer (FIDmeth), designed for detecting hydrocarbons, such as CH_4, C_2H_4, C_3H_6, as well as CO, and CO_2 up to 50%, when using helium as the carrier gas. The H_2 fraction (x_{H2}) therefore was determined by calculation with the following equations:

$$x_{H2} = 0.82(t + 273) \times 60 \times 1000 \cdot I \cdot F_{eff(H2)}/(nF\dot{V}) \qquad (11)$$

Here,

$$F_{eff\,(H2)} = 100 - \sum(F_{eff\,(1)} + F_{eff\,(2)} + \cdots F_{eff\,(n)}) \qquad (12)$$

3. Experimental

3.1 Chemicals and Materials

A PiperION anion exchange membrane (AEM) with a thickness of 40 µm was purchased from Fuel Cell Earth. Potassium bicarbonate ($KHCO_3$), Cu chloride, ammonia water, and Ir-nanoparticles, were obtained from Alfa Aesar or Milipore-Sigma Aldrich. Research-grade CO_2 was purchased from Airgas. Carbon paper and ionomer (PiperION anion exchange dispersion, 5%) were purchased from Fuel Cell Store.

3.2 Cu/GDL Cathode

Figure 1 shows a schematic drawing of electrochemical installation for synthesis of nanostructured Cu particles at porous GDL surfaces. To electroplate, a Cu-sheet is used as an anode, and carbon paper as a cathode that is attached to a Cu wire as a

lead. The cathode lead is sealed with a PTFE tape as an insulating layer to avoid unwanted side-electrochemical reaction on the Cu-lead. For the present research, we dissolved Cu salt in ammonia solution as the electrolyte. The electrolyte was prepared by 1 g $CuCl_2$, 7 ml 25% NH_3 water, 3.2 g KCl or 1 M HNO_3, and 80 ml water. Here, the KCl plays a function of supporting the electrolyte for better ionic transport. The experiment was carried out by constant current ECP at room temperature (~20 °C). The Cu^{2+} molecule forms complexes with NH_3 molecules, such as $Cu(NH_3)_2^{2+}$ or $Cu(NH_3)_4^{2+}$, depending on NH_3 water concentration and solution pH. At the anode, the Cu-metal is electro-oxidized, forming Cu-ions to enter the solution. At the cathode, the Cu-ions are electro-reduced into a Cu thin-film and deposited on the carbon paper surface. The electrode reaction is

$$Cu(NH_3)_x^{2+} + 2e^- \leftrightarrow Cu^0 + x(NH_3) \quad (13)$$

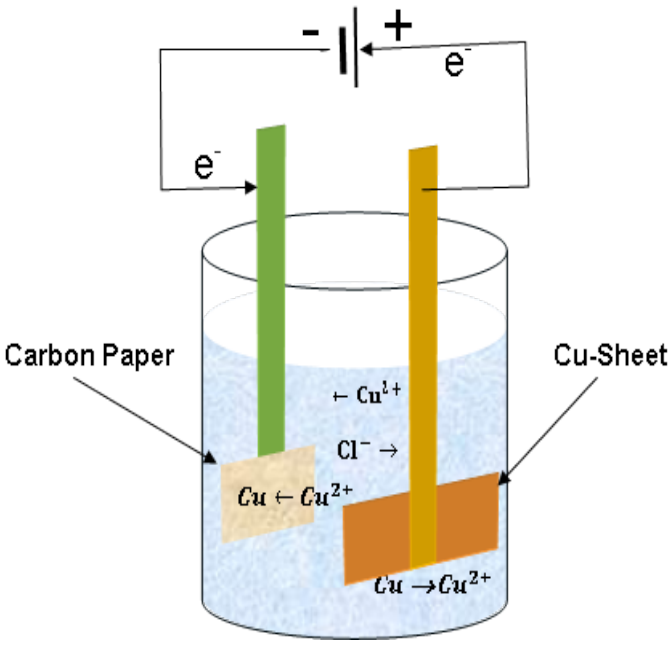

Figure 1. Schematic of electrochemical installation for synthesis of nanostructured Cu particles at porous GDL surface.

3.3 Silver Nanowires (AgNWs)

A solution (Solution 1) was prepared by dissolving 0.2 g of $AgNO_3$ in 10 mL of water and 2 mL of 25% NH_4OH in a 100 mL triangular flask, which was stirred until the $AgNO_3$ was fully dissolved. A water suspension of Cu-nanowires (Solution 2) was prepared by adding 5–10 mL of Cu-nanowire alcohol suspension (~10 mg/mL Cu) into 10 mL of water, which was stirred for 2 min. Solutions 1 and 2 were then mixed by rapid stirring. The color of the Cu-nanowires changed from golden to gray as Ag was reduced onto the surface of the Cu-nanowires. The

resulting precipitate was separated by centrifugation, washed, and dried at 60 °C in a vacuum oven.

3.4 Solid Electrolyte Interphase (SEI) with AgNWs

AgNWs (~0.012 g of catalyst) were mixed in a plastic vial with 0.3 mL water, 0.3 mL alcohol, and approximately 0.03 g of 5% PiperION ionomer. The mixture was ultrasonicated for several minutes until a uniform ink was obtained. This ink was then coated onto two pieces of 0.25-mm-thick carbon paper, each with a geometric area of 5 cm^2. After drying, the catalyst coating was visible on the carbon paper, with a total catalyst loading of approximately 1 mg/cm^2 (Ag and Cu combined), containing 90% catalyst and 10% dry ionomer.

3.5 CRT Treatment Process

The newly prepared Cu/GDL, obtained by ECP in HNO_3/KCl without subsequent washing and drying, was left exposed to air for several days until the surface turned green. Afterward, the Cu/GDL underwent chemical reduction by immersion in mixture of 0.1 M KOH and 0.1 M $NaBH_4$ at 80 °C for 10 min, followed by washing and assembly into an MEA cell for CO2RR testing.

3.6 Anode Preparation

Anode ink of iridium (Ir)-nanoparticles was made by weighing 0.040 g Ir-nanoparticles in a plastic vial, adding 0.3 mL water, 0.3 mL alcohol, and 0.34 g 5% PiperION anion exchange dispersion ionomer. The vial was ultrasonicated for 5–10 min until it formed a uniform ink. The ink was coated on four pieces of 0.25-mm-thick 5 cm^2 carbon paper. After it was dried, a catalyst coating formed on the carbon paper, with a catalyst loading of 2 mg/cm^2, containing 70% catalyst and 30% dry ionomer.

3.7 AEM

A PiperION AEM with a thickness of 40 μm was tailored to 6.5 × 6.5 cm for each MEA preparation. It was soaked in water for more than 1 h before using.

3.8 Electrochemical Reactor and Test Platform

The cathode, membrane, and anode were sandwiched together to form an MEA in electrolyzer hardware that had two graphite plates to hold the MEA. Gas and liquid flow channels were engineered on the inner phase of the graphite plates that were facing the outer phase of the MEA. CO_2 gas was passed through the cathode flow

channel, and water or electrolyte was passed through the anode flow channel. Figure 2 shows a flow diagram of CO_2 electrochemical reduction and the zero-gap reactor's structure. We used a gas regulator to apply a small pressure (20–40 psi) of CO_2, as input to a mass flow control (MFC). We inserted the MFC between the gas regulator and the humidifier to accurately control the input CO_2 gas flow rate into the reactor. After being humidified, the CO_2 gas flowed into the cathode side of the reactor. The products from CO2RR were passed through a water trap to remove water vapor. A mass flow meter (MFM) was installed after the water remover to measure the flow rate of the outlet gas products, since the gas flow rate changed with time after the reaction. The gas flow-rate data from the MFM were used as the actual flow rate for GC analysis and calculation of electrochemical parameters. Gas product samples from the reactor were taken periodically to determine the gas fractions with a GC. Furthermore, a small mechanic circulation pump was added in the CO2RR test platform between the anode flow channel and electrolyte container that enabled a wide range of anode electrolytes. The CO2RR test platform after optimization has the advantages of evaluating MEAs by varying gas flow rate, cell temperature, and electrolytes. To obtain CO2RR performance with cell temperature, a thermocouple and heaters were inserted in the Cu holder of the reactor to automatically control the temperature of the cell with a computer. The sealing frames in the reactor are optimized to match the thickness of the MEA, which has an approximately equal thickness of the sum of the membrane, catalyst layers, and GDLs. The electrochemical measurements were performed with an Arbin Instruments battery tester with MIT Pro8 software and a Keysight E3633A DC power supply.

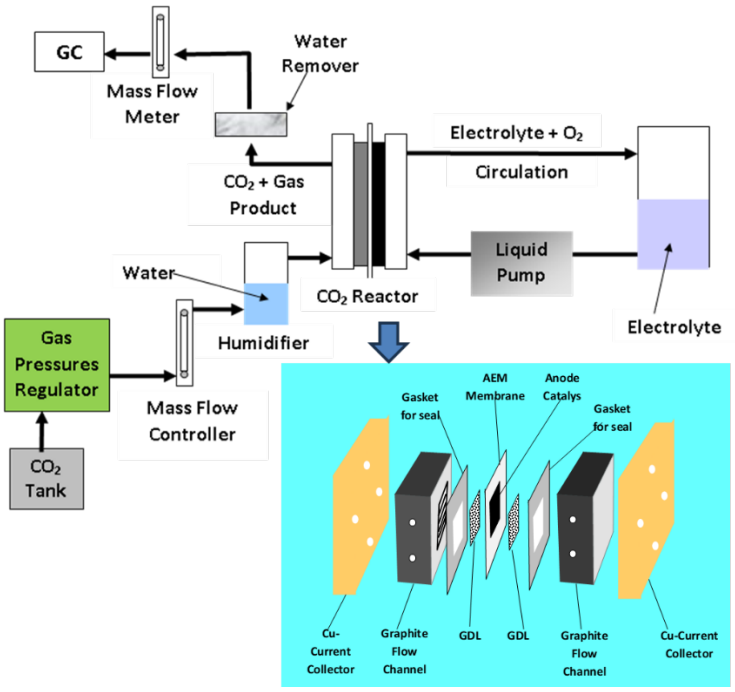

Figure 2. Flow diagram of CO_2 electrochemical reduction and the zero-gap reactor's structure.

3.9 MEA Pretreatment Before Test

Before each electrochemical measurement, the reactor was pretreated at 60 °C by circulation of water or electrolyte through the anode channel, or through the cathode channel, or both, depending on individual experiments. As the cell performance was increasing with operational and pausing time, the cell was tested several times, and the best results were reported.

3.10 Gas Product Analysis

An SRI 8610C GC was used for analysis of CO2RR gas products from the electrochemical reactor. It contains an FID with a methanizer to increase its sensitivity, and a thermal conductivity detector.

3.11 Materials Characterization

A Malvern Panalytical XPert 3 was used for X-ray diffraction (XRD) analysis, with a Cu Kα source and parabolic mirror for incident optics, and a parallel-plate collimator for receiving optics. A Zeiss Auriga scanning electron microscope was used at an accelerating voltage of 15 kV for analyzing morphology with scanning electron microscopy (SEM), with an attached Ametek EDAX energy-dispersive X-ray spectroscopy (EDS) for spatial elemental analysis.

4. Results and Discussion

4.1 Concept of SEI layer, Single Functional GDL, and Bifunctional GDL for ECP

We used porous carbon paper as a GDL to load the Cu-nano catalyst for CO2RR. The GDL was treated with PTFE (from 5% to 40%) to increase the surface hydrophobicity, subsequently allowing faster CO_2 gas transport through its micropores. Due to the hydrophobicity at the PTFE-containing carbon paper surface, the Cu-ions are unable to directly approach and be adsorbed for ECP. Therefore, we applied a hydrophilic SEI layer on the GDL to mediate the electrochemical deposition. To make the SEI layer, a short-chain ionomer was coated onto the GDL surface, which became a cohesive layer after the solvent evaporated. In this study, we used a PiperION ionomer with and without doping AgNWs as the SEI layer on GDL. Figure 3 shows a conceptual graphic of the SEI layer, hydrophobic GDL, and bifunctional GDL for ECP. The original carbon paper is noted as "single functional GDL" because of its hydrophobic activity. After covering the GDL with an SEI layer, it becomes a "bifunctional GDL" that has both a hydrophobic bottom layer and hydrophilic top layer. Table 1 details the preparation conditions for the following experiments.

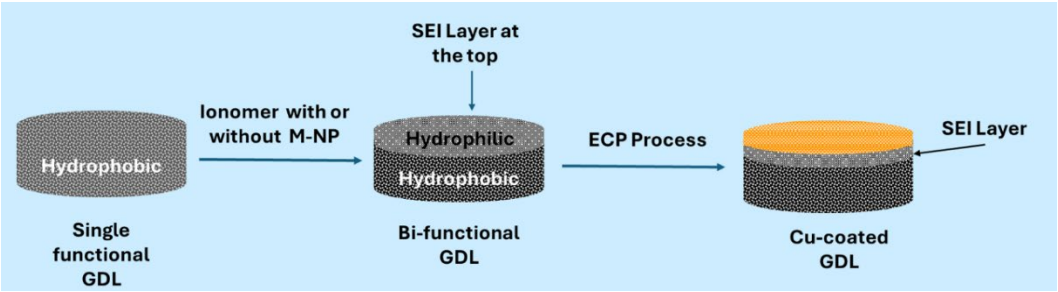

Figure 3. Concept of SEI layer, hydrophobic GDL, and bifunctional GDL for ECP of Cu-thin film on GDL as the CO2RR catalyst.

Table 1. ECP conditions for 5 cm^2 carbon paper cathodes.

Deposition name	SEI	ECP current density (mA/cm^2)	ECP charge deposited (mAh)	CRT
ECP-a	Undoped	5	64	×
ECP-a-high	Undoped	25	50	×
ECP-b	AgNW-doped	5	50	×
ECP-c	AgNW-doped	1	89	×
ECP-d	Undoped	10	120	✓

4.2 CO2RR Performance at Cu/GDL with Undoped SEI Layer

Figure 4 shows CO2RR results obtained from the alkaline MEA reactor. The ECP-a cathode electrode was prepared by ECP of a thin layer of Cu on 0.25-mm-thick 5 cm^2 carbon paper. There are three key factors in the ECP process: ECP current density, ECP capacity, and SEI layer, which all play an important role in Cu-coating quality, crystal size, and morphology, as well as catalytic activity, selectivity, and stability for CO2RR. Here, we control current at 25 mA for the ECP process, or 5 mA/cm^2 current density, with an end-reaction charge capacity of 64 mAh, or 12.8 mAh/cm^2. The SEI layer is pure (100%) PiperION ionomer. This configuration of parameters is labeled ECP-a. The MEA with an ECP-a cathode gives excellent C_2H_4 selectivity for CO2RR in all operating temperatures. At 20 °C, the F_{eff} reaches to 79% for C_2H_4 and 87.5% for total CO2RR. Even at 60 °C, the F_{eff} is 39.5% for C_2H_4 and 60% for total CO2RR. High catalytic activity is also obtained by calculation of individual product catalytic current density (Figure 4d). At 60 °C, the individual product current density is 131.5 mA/cm^2 for C_2H_4, and 199.7 mA/cm^2 for total CO2RR. Figure 5 shows a GC obtained from the outlet gas sample of this MEA reactor for CO2RR. A high C_2H_4 peak is demonstrated.

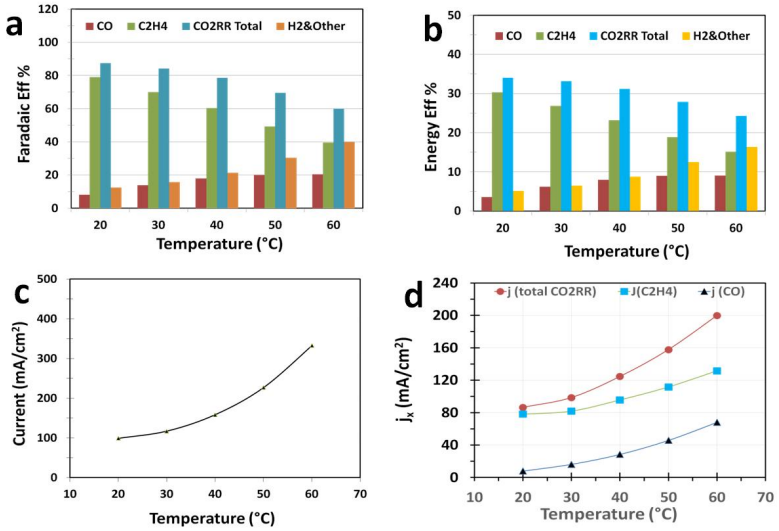

Figure 4. CO2RR results obtained from an alkaline MEA reactor with an ECP-a cathode: ECP current 25 mA; ECP capacity 64 mAh; and SEI layer PiperION. (a) F_{eff}, (b) E_{eff}, (c) total cell current density, and (d) calculated current density of j_x (here, x means total CO2RR, CO, and C_2H_4 products). Cell voltage: 3.0 V.

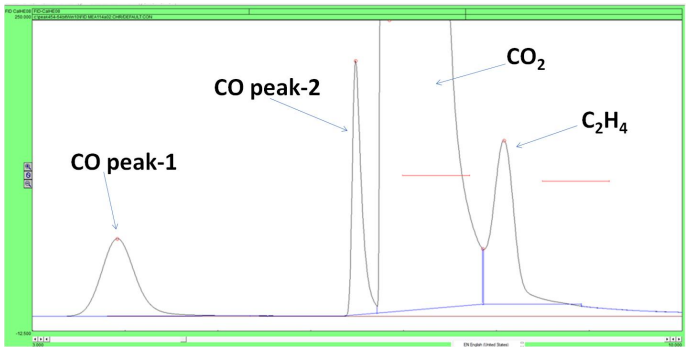

Figure 5. GC obtained from the outlet gas sample of an MEA reactor with ECP-a cathode that is shown in Figure 4 operating at 20 °C, 3.0 V, MFC set to 60 sccm, and MFM measuring 51 sccm.

By varying the ECP deposition conditions to make the Cu/GDL electrode, the MEA reactor CO2RR performance was correspondingly changed. Figure 6 shows CO2RR results obtained from an alkaline MEA reactor, where the cathode electrode was prepared by controlling ECP condition at higher current density (25 mA/cm^2), or 125 mA for a 5 cm^2 carbon paper as the cathode, "ECP-a-high."

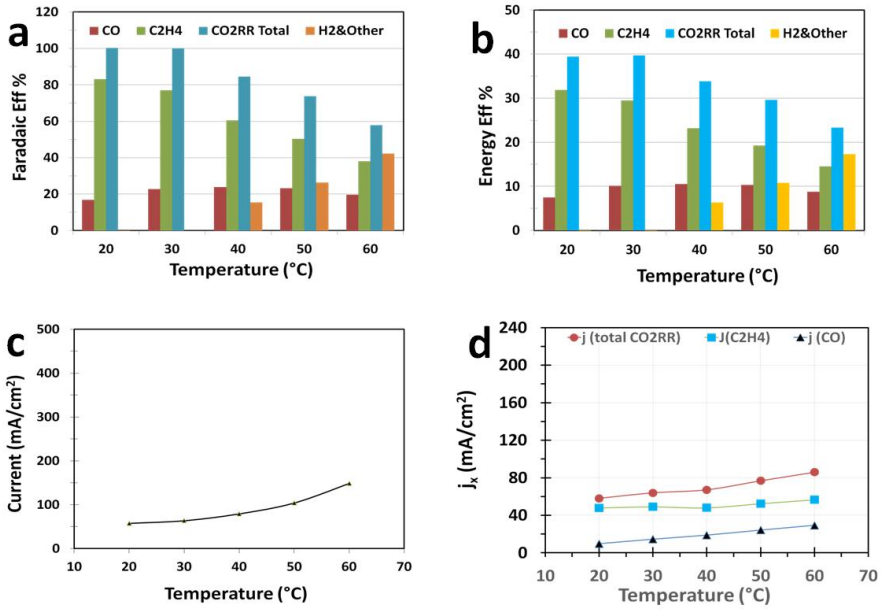

Figure 6. CO2RR results obtained from an alkaline MEA reactor with an ECP-a cathode: ECP current 100 mA; ECP capacity 50 mAh; and SEI layer PiperION. (a) F_{eff}, (b) E_{eff}, (c) total cell current density, and (d) calculated current density of j_x (here, x means total CO2RR, CO, and C_2H_4 products). Cell voltage: 3.0 V.

The F_{eff} of the ECP-a-high sample reached 83% for C_2H_4, and a total CO2RR of nearly 100%, or no H_2 product is detected at 20 °C and 3.0 V operating conditions. The corresponding E_{eff} for total CO2RR was 39% at 20–30 °C operating temperatures. However, the individual product current density was not high–only

56.5 mA/cm^2 for C_2H_4 and 86 mA/cm^2 for the total CO2RR. This was far less than the values of 131.5 mA/cm^2 for C_2H_4, and 199.7 mA/cm^2 for total CO2RR, that were obtained with ECP-a by controlling the ECP current density at 5 mA/cm^2. It seems that controlling ECP operating conditions at higher current density turned out better C_2H_4 product selectivity, but lower individual product current density.

To better understand the effects of the ECP deposition current density on the above results, XRD and SEM were used to evaluate the nature of the deposited Cu. As shown in Figure 7, the symmetric 2θ-ω XRD scan showed the two characteristic peaks of Cu; namely, the Cu (111) peak at 43.3° and the Cu (002) peak at 50.4°. Apart from the graphite (004) peak resulting from the porous carbon GDL substrate, there existed no phases indicative of other elements present, thus confirming that the ECP deposition process results in face-centered cubic Cu without other phases indicative of other elements.

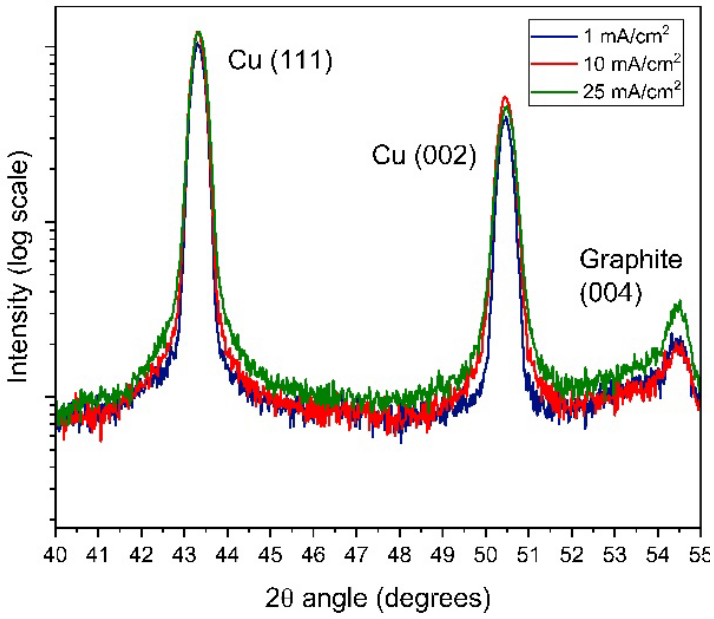

Figure 7. Symmetric 2θ-ω XRD scans of ECP Cu on porous carbon at various deposition currents.

SEM images of the ECP Cu at different currents, however, showed distinct morphologies of the Cu deposition on the bifunctional GDL. As compared with a bare porous carbon substrate shown in Figure 8a, lower deposition current densities (1 mA/cm^2, shown in Figure 8b) produced a rough and nonconformal Cu deposition on the GDL; instead of a film, the Cu formed as connected nodules. As the current density is increased, the morphology was more conformal (5 mA/cm^2, shown in Figure 8c; 25 mA/cm^2, shown in Figure 8d), with the Cu features matching the features of the bare porous carbon substrate. A closer comparison of the ECP Cu deposited at 5 mA/cm^2 versus 25 mA/cm^2 showed that more of the bifunctional

GDL was exposed at the lower current due to less conformal coverage. Additionally, the Cu surface morphology was rougher at the 5 mA/cm^2 deposition current, with noticeable bumps along the lines of Cu.

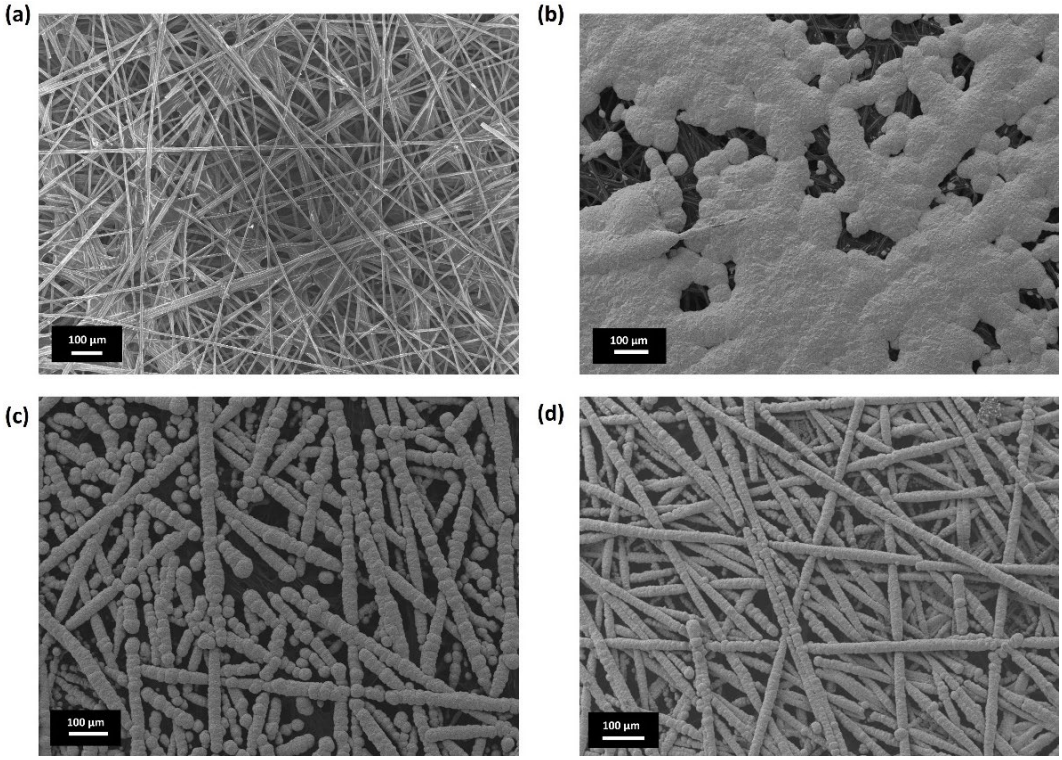

Figure 8. SEM images of (a) bare porous carbon, which matches the morphology of the bifunctional GDL; (b) ECP Cu deposited at a current density of 1 mA/cm^2; (c) ECP Cu deposited at a current density of 5 mA/cm^2; and (d) ECP Cu deposited at a current density of 25 mA/cm^2.

To confirm that the higher ECP deposition current density blocked out more of the bifunctional GDL layer, EDS was performed on ECP Cu at the three different current conditions (1 mA/cm^2, 5 mA/cm^2, and 25 mA/cm^2), with the results shown in Figure 9. For the lowest current, the most carbon (representing the bifunctional GDL) was exposed, while for the highest current, the least carbon was exposed. For the images of ECP Cu deposited at 25 mA/cm^2, an area was selected that was the boundary of the deposition; the exposed carbon was masked off with the PTFE tape at the cathode for the ECP process. When specifically analyzing the areas where there was deposited Cu, there was virtually no exposed bifunctional GDL material at 25 mA/cm^2 ECP deposition, whereas there was some at 5 mA/cm^2.

The difference between the product selectivity and current density between ECP-a and ECP-a-high can be explained by this relative exposure of the bifunctional GDL compared with Cu. ECP-a had less selectivity toward C_2H_4 production, since some of the exposed bifunctional GDL electrochemical area that was not Cu-coated was

driving hydrogen evolution as a cathode reaction; conversely, this exposed bifunctional GDL area was facilitating better diffusion kinetics of the reactants with the dual hydrophilic/hydrophobic engineering, which produced a higher overall product current density. By a similar argument, ECP-a-high had high selectivity toward C_2H_4 production, since the entirety of the electrochemical area was Cu-coated without any exposure of the bifunctional GDL; conversely, since the ECP Cu was completely covering the bifunctional GDL in the active electrochemical area, the reactant diffusion kinetics were reduced, causing a lower overall product current density.

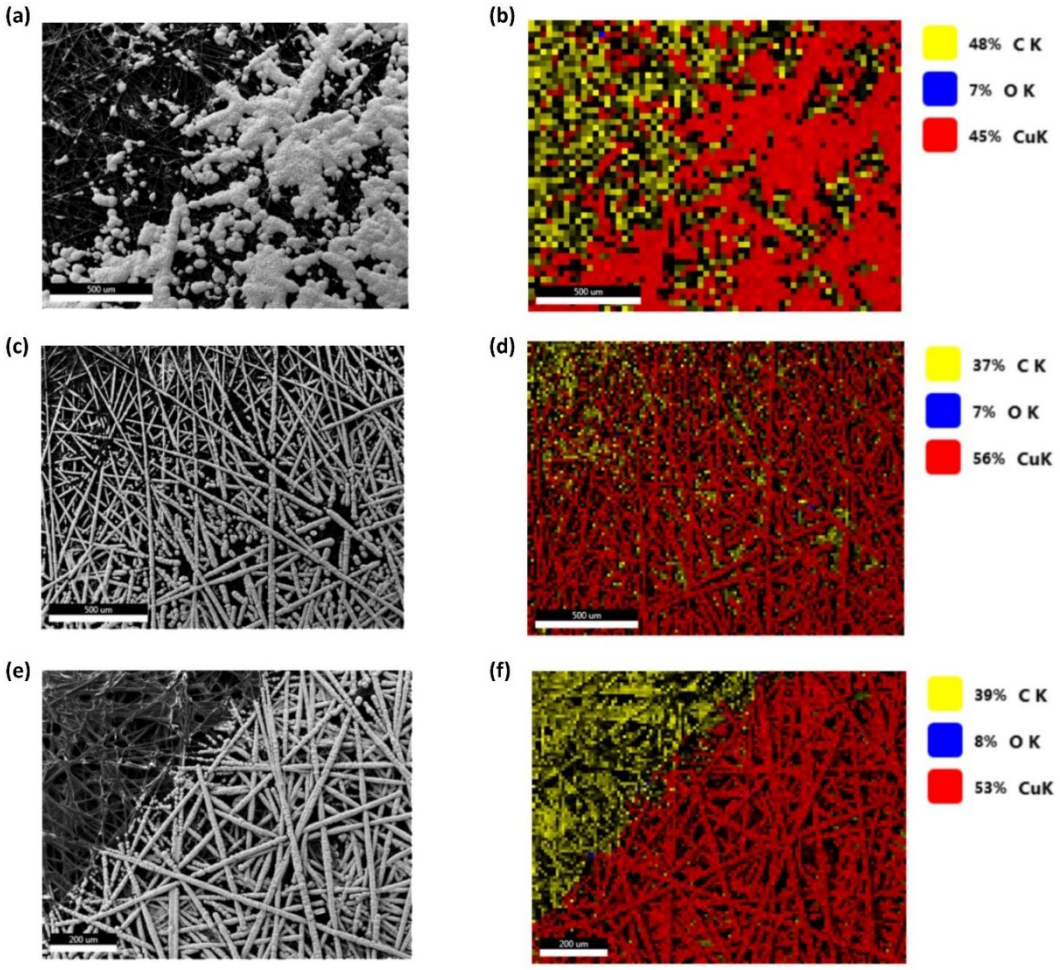

Figure 9. SEM images with corresponding EDS maps of carbon, oxygen, and Cu of (a, b) ECP Cu deposited at a current density of 1 mA/cm^2; (c, d) ECP Cu deposited at a current density of 5 mA/cm^2; and (e, f) ECP Cu deposited at a current density of 25 mA/cm^2.

4.3 CO2RR Performance at Cu/GDL with AgNW-doped SEI Layer

The SEI layer played an important role in the ECP process to attach Cu-nano particles on the porous GDL surface. To observe the impact of the SEI layer on the Cu/GDL on CO2RR performance, we incorporated AgNWs into the ionomer (PiperION). Figure 10 shows CO2RR results obtained from the alkaline MEA reactor. The cathode electrode was prepared by ECP with a thin layer of Cu on 0.25-mm-thick 5 cm^2 carbon paper with AgNW/PiperIon as the SEI layer. The ECP current density was controlled at 5 mA/cm^2, or 25 mA current for a 5 cm^2 Cu/GDL electrode, ECP-b. At 20 °C and 3.0 V operating conditions, the MEA gave a high F_{eff} of 76.4% for C_2H_4 and 89.5% for total CO2RR. At 60 °C and 3.0 V, a high F_{eff} ratio of C_2H_4 versus CO was still maintained, or 21.5% for C_2H_4 and 2.9% for CO. However, the individual product current density for CO2RR is not high, as shown in Figure 10d. The peak current density for C_2H_4 product was only 83 mA/cm^2 at 50 °C, 3.0 V operating conditions. Figure 11 shows a GC obtained from the outlet gas sample of this MEA reactor with an ECP-b cathode for CO2RR. A high C_2H_4 peak is seen.

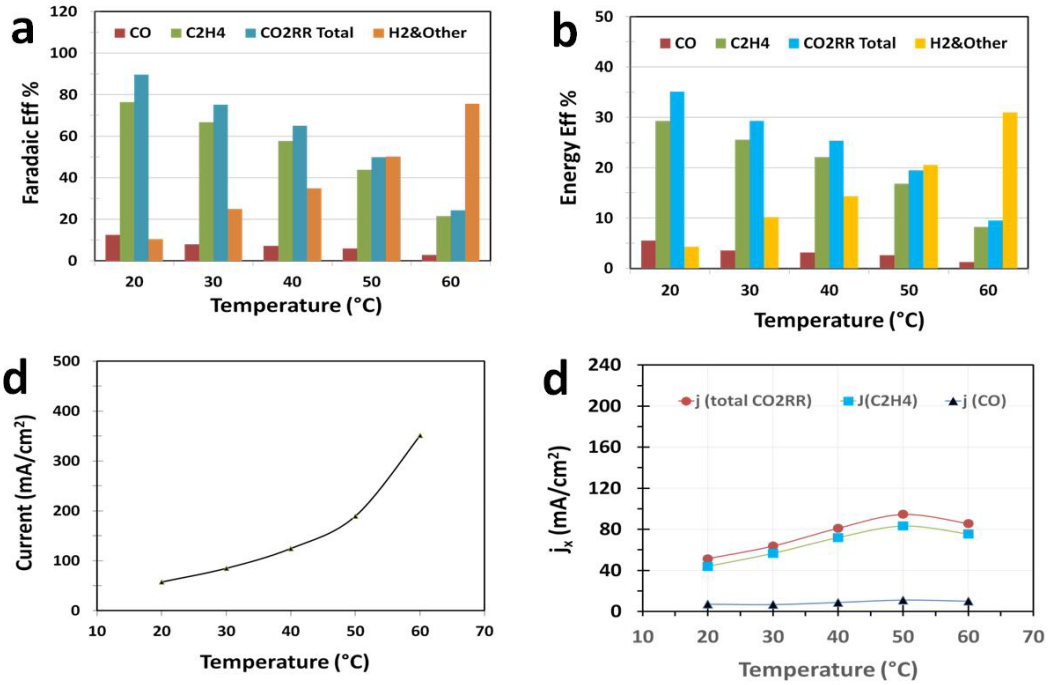

Figure 10. CO2RR results obtained from an alkaline MEA reactor with an ECP-b cathode: ECP current 25 mA, ECP capacity 50 mAh, and SEI layer is AgNW/PiperION. (a) F_{eff}, (b) E_{eff}, (c) total cell current density, and (d) calculated current density of j_x (here, x means total CO2RR, CO, and C_2H_4 products). Cell voltage: 3.0 V.

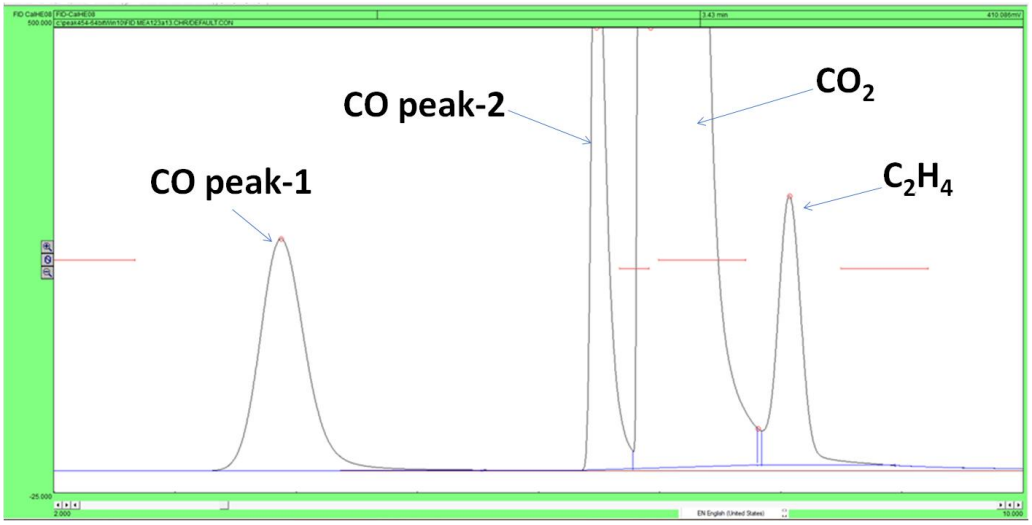

Figure 11. GC obtained from the outlet gas sample of an MEA reactor that is shown in Figure 10 operating at 60 °C, 3.0 V, MFC set at 30 sccm, and MFM measuring 24.5 sccm.

To achieve high current densities from individual CO2RR products, we lowered the ECP current density to 1 mA/cm^2 to prepare the Cu/GDL. Figure 12 shows CO2RR results obtained from the alkaline MEA reactor. The cathode electrode was prepared by ECP with a thin layer of Cu on 0.25-mm-thick carbon paper with AgNW/PiperION as the SEI layer, ECP-c. Surprisingly, the F_{eff} ratio of C_2H_4 versus CO changed significantly compared with the 5 mA/cm^2 sample, which is likely related to CO_2 direct reduction at the AgNW surfaces, as Ag is a good catalyst for CO2RR to CO. At 20 °C and 3.0-V operating condition, the F_{eff} is 15% for C_2H_4, and 58.9% for CO, with total CO2RR F_{eff} of 73.9%. Interestingly, the individual product current density increased, as shown in Figure 12d, to 120.5 mA/cm^2 for C_2H_4 and 146.8 mA/cm^2 for total CO2RR at 60 °C, 3.0 V operating conditions. These results are also explained by the amount of exposed bifunctional GDL area at the low ECP deposition current of 1 mA/cm^2. As evidenced by Figures 10a, 12a, and 12b, ECP-c has less selectivity toward C_2H_4 production and an increased component of hydrogen evolution, since some of the exposed bifunctional GDL electrochemical area that is not Cu-coated is driving hydrogen evolution as a cathode reaction; conversely, this exposed bifunctional GDL area is facilitating better diffusion kinetics of the reactants with the dual hydrophilic/hydrophobic engineering, which produces a higher overall product current density.

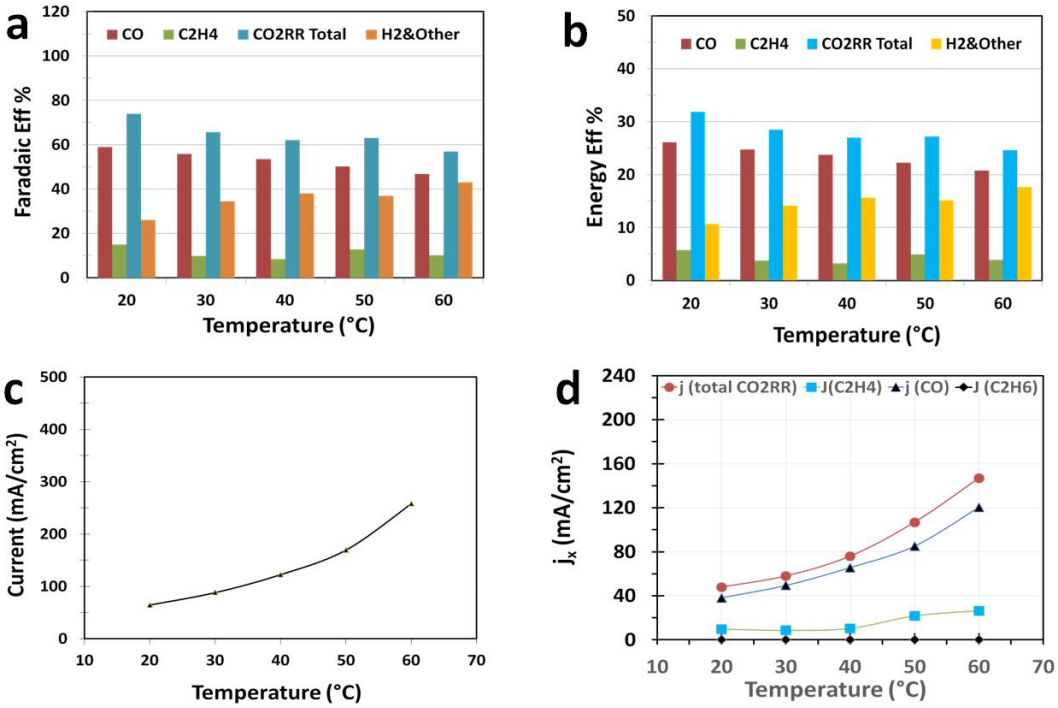

Figure 12. CO2RR results obtained from an alkaline MEA reactor with an ECP-c cathode: ECP current 5 mA, ECP capacity 89 mAh, and SEI layer is AgNW/PiperION. (a) F_{eff}, (b) E_{eff}, (c) total cell current density, and (d) calculated current density of j_x (here, x means total CO2RR, CO, and C_2H_4 products). Cell voltage: 3.0 V.

4.4 CO2RR Performance at Cu/GDL by CRT

The electrode surface area is highly related to its surface roughness. Therefore, we explored a method to enhance the Cu/GDL surface area by CRT of the Cu/GDL electrode to increase its catalytic activity and selectivity for CO2RR. After the CRT process, the Cu/GDL demonstrated high activity and selectivity when it was used as a cathode for CO2RR in an alkaline MEA reactor. Figure 13 shows CO2RR results of a Cu/GDL prepared by ECP process and followed by CRT treatment, ECP-d. It showed exceptionally high current density, reaching approximately 1000 mA/cm^2 (Figure 13c). As a large fraction of the current was from HER, the F_{eff} for CO2RR was not high, reaching only 52% for total CO2RR, 41% for C_2H_4, and 7% for CO at 20 °C operating temperature. However, the F_{eff} for C2 products (C_2H_4 + C_2H_6) was about 6 times larger than that of the C1 product (CO). Figure 14 shows the GC obtained from the outlet gas sample of the MEA reactor that is shown in Figure 13 operating at 50 °C. A large C_2H_4 peak was seen with a larger peak area than that of CO, which is consistent with a high F_{eff} ratio of C_2H_4 to CO (Figure 13a).

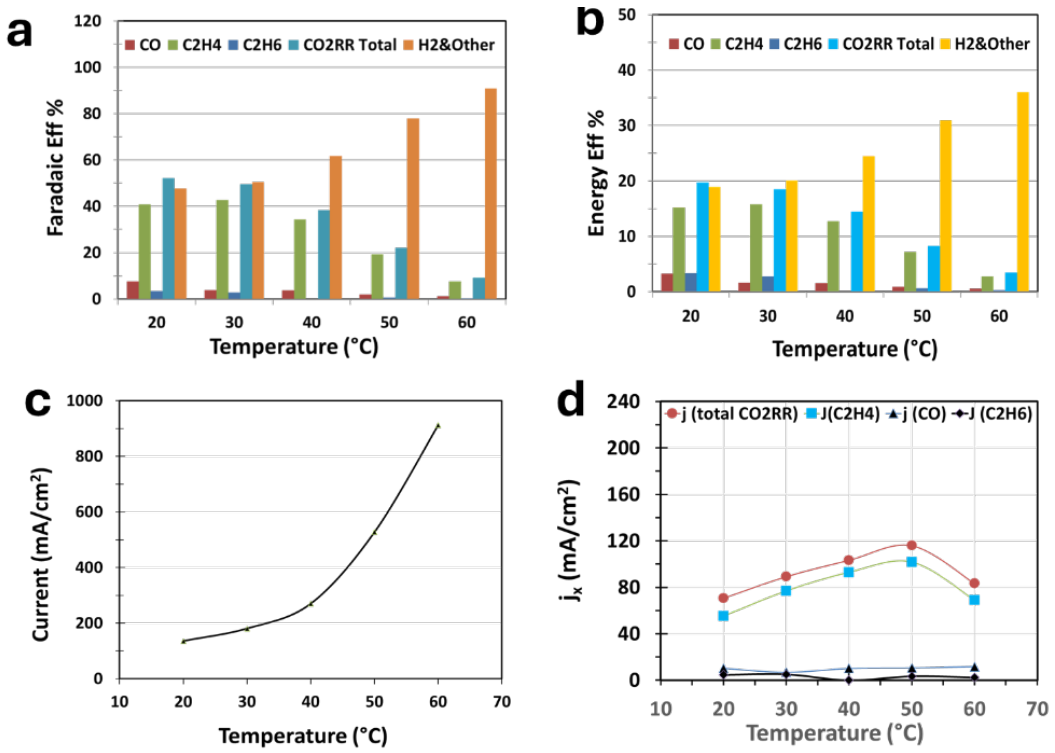

Figure 13. CO2RR results of a Cu/GDL prepared by ECP process and followed by CRT treatment, ECP-d. ECP current 50 mA, ECP capacity 120 mAh, and SEI layer is PiperION. (a) F_{eff}, (b) E_{eff}, (c) total cell current density, and (d) calculated current density of j_x (here, x means total CO2RR, CO, and C_2H_4 products). Cell voltage: 3.1 V.

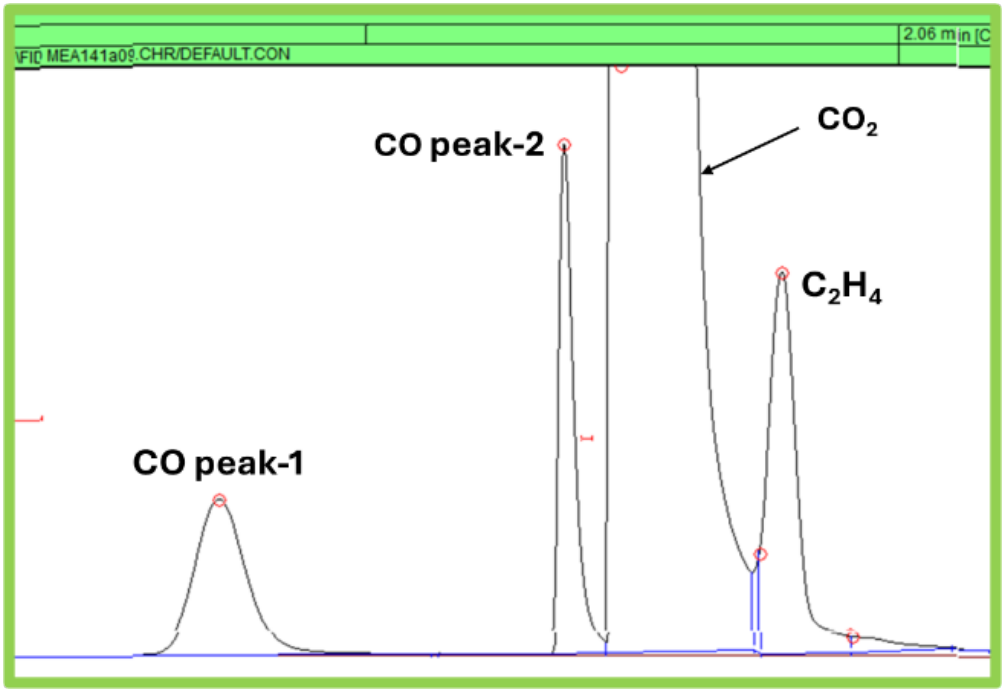

Figure 14. GC obtained from the outlet gas sample of an MEA reactor that is shown in Figure 13 operating at 50 °C, 3.0 V, MFC at 60 sccm, and MFM at 57.8 sccm.

To give insight to how CRT affected the ECP Cu, both XRD and SEM measurements were performed, with the results shown in Figure 15. The ECP Cu underwent some amount of oxidation, as evidenced by the emergence of the Cu_2O (111) and (220) peaks in the symmetric 2θ-ω XRD scan (Figure 15a). The SEM images shown in Figures 15b and 15c showed a total loss of the conformal ECP Cu morphology when initially evaluated (Figure 8). Instead of connected nodules in the case of low deposition current, or conformal films with higher deposition current, the Cu morphology had the form of a cracked film that can be thought of as a series of connected platelets. A zoomed-in view, as shown in Figure 15c, showed microscale (and perhaps nanoscale) roughening. Due to the CRT process being a long ambient-air oxidation with a subsequent short chemical reduction, the presence of Cu_2O is indicative of the chemical reduction not fully re-reducing the initial ECP Cu, either from the limited time of the reduction to not fully react with all the present Cu_2O, or from the limited diffusion of reducing chemical species within the porous carbon to access all oxidized material. The SEM images confirm an in-situ roughening effect from converting Cu_2O back to Cu that increased the active surface area for catalytic sites and improved catalysis properties and can help explain the high current density and high selectivity for C2 products at high overpotentials; similar results have been reported from Cu foils being oxidized through air annealing and then electrochemically reduced.[20]

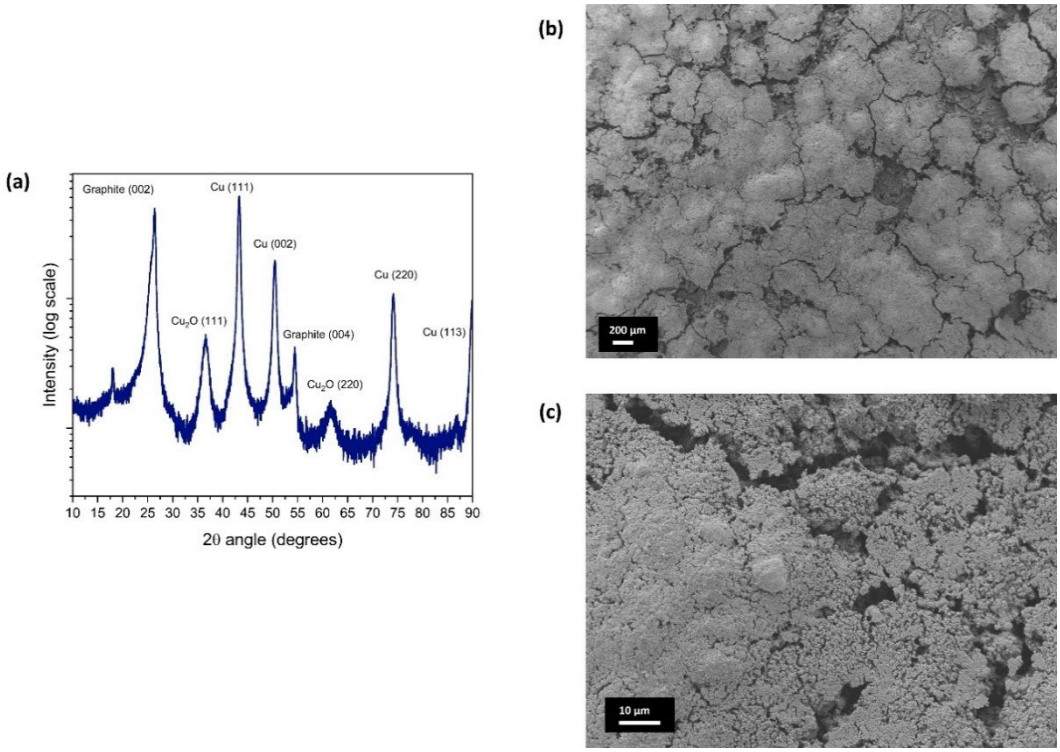

Figure 15. Materials characterization of ECP Cu after CRT treatment: (a) symmetric 2θ-ω XRD scan; SEM images of surface morphology (b) zoomed out, and (c) zoomed in.

4.5 Comparison of Gas Yield Rates Between Different Cu/GDL Preparation Conditions by ECP Method

The mechanisms of CO2RR are complex, and may result in various products, such as CO, CH_4, and HCOOH (C1 products), C_2H_2, C_2H_4, C_2H_6, C_2H_5OH, and CH_3COOH (C2 products), and C_3H_6, and C_3H_8 (C3 products). In addition, we encountered a large amount of side reaction (HER) in the process of CO2RR with a zero-gap MEA reactor. To convert CO_2 to an energy-dense fuel by electrochemical methods, we controlled the product selectivity by multiple methods, not only the catalyst, but also the catalyst preparation conditions.

Here, we compare the effects of different ECP conditions on C_2H_4 selection for CO2RR with a zero-gap alkaline MEA reactor. Figure 16 shows the gas yield rate of CO2RR from alkaline MEA reactors that used Cu/GDL as the cathodes prepared by ECP method with different synthetic conditions.

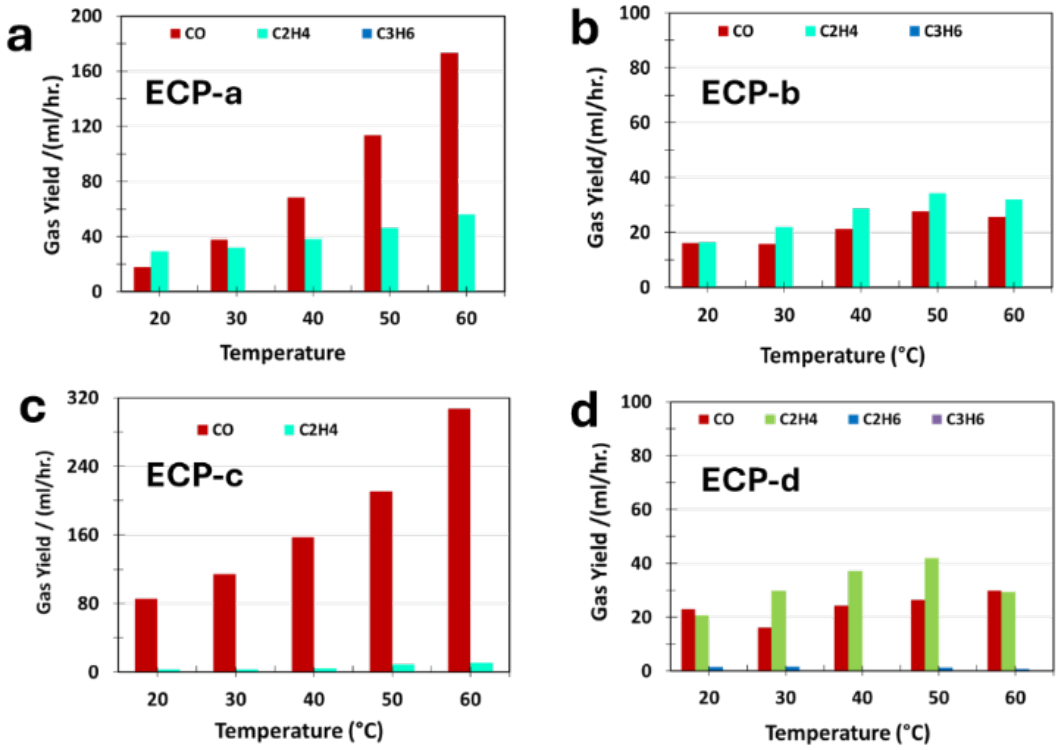

Figure 16. Gas yield rate of CO2RR from zero-gap alkaline MEA reactors that use Cu/GDL as the cathodes prepared by ECP method with different synthetic conditions. (a) ECP-a, Cu/GDL with undoped SEI layer, ECP current 25 mA; (b) ECP-b, Cu/GDL with AgNW-doped SEI layer, ECP current 25 mA; (c) ECP-c, Cu/GDL AgNW-doped SEI layer, ECP current 5 mA, and (d) ECP-d, Cu/GDL treated with CRT method.

The CO2RR performance obtained from the ECP-a condition, where the Cu/GDL was prepared with undoped SEI layer at a current of 25 mA, demonstrated excellent F_{eff} (87.5% at 20 °C) and current density (~200 mA/cm^2 at 60 °C) for total CO2RR,

as shown in Figures 4a and 4d. However, by further GC analysis of the gas product, the majority gas was CO (173 ml/h at 60 °C). The flux of C_2H_4 is only 55.9 ml/hr (at 60 °C), and the overall gas flux ratio of C_2H_4/CO was only 0.32. The gas flux ratio changed by varying the ECP conditions. For the ECP-b condition, where the Cu/GDL was prepared with AgNW doped SEI layer at current 25 mA, the gas flux of C_2H_4/CO (32%/25.7%) increased to 1.25, although it had a smaller current density (94.5 mA/cm^2 at 60 °C) of total CO2RR, as shown in Figure 10d. The CO2RR performance was also changed by varying the ECP current for preparation of Cu/GDL. Figure 16c shows gas flux rate of CO2RR obtained from the Cu/GDL prepared by ECP-c condition, where the Cu/GDL was prepared with AgNW-doped SEI layer at current 5 mA (1 mA/cm^2), the CO product flux (at 60 °C) reached to 307 ml/hr, and the C_2H_4 flux was only 11 ml/hr, which turned out the ratio of C_2H_4/CO was only 0.036. Figure 16d shows gas flux rate of CO2RR obtained from the Cu/GDL prepared by ECP-d condition, where the Cu/GDL was prepared by corrosion treatment, the highest ratio of C_2H_4/CO at 50 °C was obtained (1.6). These experimental results demonstrate that the fraction of C_2H_4 product versus CO can be adjusted by varying the ECP condition for preparation of Cu/GDL; therefore, we can increase the C2 product ratio for energy-dense fuel.

5. Conclusion

In this research we demonstrated methods to efficiently convert CO_2 to energy-dense fuels using hybrid electrochemical technologies, including synthesis of Cu-thin film catalysts on GDLs by ECP, electrode surface optimization by CRT and advanced zero-gap reactor design with an alkaline membrane electrode assemble (MEA). At low operating temperatures (20–30 °C) and 3.0 V cell voltage, the F_{eff} reached up to 83% for C_2H_4 and nearly 100% for total CO2RR. At high temperatures (60 °C) and 3.0 V cell voltage, the product current density reached 131 mA/cm^2 for C_2H_4 and nearly 200 mA/cm^2 for total CO2RR. The gaseous fuels generated from the reactor were further analyzed with a GC and plotted by fuel gas yield rate versus reactor operating conditions. The ratio of energy-dense fuel (C_2H_4) to low energy fuel (CO) was highly dependent on ECP conditions for preparation of Cu/GDL cathode electrode and ranged from 0.036 (CO rich) to 1.6 (C_2H_4 rich), depending on the ECP condition. The C2 product ratio for energy-dense fuel was highest using the CRT technique and without AgNW dopant in the SEI layer, while the lowest ratio was without CRT and with AgNWs doped in the SEI. Undoped SEI layers demonstrated the highest C_2H_4 yields overall, implying that AgNWs may not be necessary for overall C_2H_4 generation, but the high CO content or high H_2 content generated by these formulations would need a further purification step for C_2H_4 isolation.

6. References

1. Nitopi S et al. Progress and perspectives of electrochemical CO2 reduction on copper in aqueous electrolyte. Chem Rev. 2019;119:7610−7672.
2. Xiao C, Zhang J. Architectural design for enhanced C2 product electivity electrochemical CO2 reduction using cu-based catalysts: a review. ACS Nano. 2021;15:7975−8000.
3. Bui JC et al. Engineering catalyst−electrolyte microenvironments to optimize the activity and selectivity for the electrochemical reduction of CO2 on Cu and Ag. Acc Chem Res. 2022;55:484−494.
4. Overa S, Ko GH, Zhao Y, Jiao F. Electrochemical approaches for CO2 conversion to chemicals: a journey toward practical applications. Acc Chem Res. 2022;55:638−648.
5. Guan YY, Liu YY, Yi J, Zhang JJ. Zeolitic imidazolate framework-derived composites with SnO2 and ZnO phase components for electrocatalytic carbon dioxide reduction. Dalton Transactions. 2022;51:7274−7283.
6. Yin Z et al. Hybrid catalyst coupling single-atom Ni and nanoscale Cu for efficient CO2 electroreduction to ethylene. J Am Chem Soc. 2022;144:20931−20938.
7. Wang S et al. Industrial-level CO2 electroreduction using solid-electrolyte devices enabled by high-loading nickel atomic site catalysts. Adv Energy Mater. 2022;12:2201278.
8. Chu S et al. Photoelectrochemical CO2 reduction into syngas with the metal/oxide interface. J Am Chem Soc. 2018;140:7869−7877.
9. Wang Y et al. Dramatic enhancement of CO2 photoreduction by biodegradable light-management paper. Adv Energy Mater. 2018;8:1703136.
10. Lei Q et al. Investigating the origin of enhanced C2+ selectivity in oxide/hydroxide-derived copper electrodes during CO2 electroreduction. J Am Chem Soc. 2020;142:4213−4222.
11. Ni Z et al. Research progress of electrochemical CO2 reduction for copper-based catalysts to multicarbon products. Coord Chem Rev. 2021;441:213983.

12. Lai Y et al. Breaking scaling relationships in CO2 reduction on copper alloys with organic additives. ACS Cent Sci. 2021;7:1756−1762.

13. Wei X et al. Highly selective reduction of CO2 to C2+ hydrocarbons at copper polyaniline interfaces. ACS Catal. 2020;10:4103−4111.

14. Hahn C et al. Engineering Cu surfaces for the electrocatalytic conversion of CO2: controlling selectivity toward oxygenates and hydrocarbons. PNAS. 2017;114:5918−5923.

15. Arquer FPD et al. CO2 electrolysis to multicarbon products at activities greater than 1 A cm−2. Science. 2020;367:661−666.

16. Larrazábal GO et al. Analysis of mass flows and membrane cross-over in CO2 reduction at high current densities in an MEA-type electrolyzer. ACS Appl Mater Interfaces. 2019;11:41281−41288.

17. Vázquez MJG et al. Environment matters: CO2RR electrocatalyst performance testing in a gas-fed zero-gap electrolyzer. ACS Catal. 2020;10:13096−13108.

18. Yin Z et al. An alkaline polymer electrolyte CO2 electrolyzer operated with pure water. Energy Environ Sci. 2019;12:2455−2462.

19. Guo L et al. Electroplated copper additives for advanced packaging: a review. ACS Omega. 2024;9:20637−20647.

20. Li CW, Kanan MW. CO_2 reduction at low overpotential on Cu electrodes resulting from the reduction of thick Cu_2O films. JACS. 2012;134:7231−7234.

List of Symbols, Abbreviations, and Acronyms

AEM	anion exchange membrane
AgNW	silver nanowire
C_2H_4	ethylene
CO	carbon monoxide
CO_2	carbon dioxide
CO2RR	CO_2 reduction reaction
CRT	corrosion/reduction treatment
Cu	copper
DC	direct current
ECP	electrochemical plating
EDS	energy-dispersive X-ray spectroscopy
E_{eff}	energy efficiency
F_{eff}	Faradaic efficiency
FID	flame ionization detector
GC	gas chromatograph
GDL	gas diffusion layer
HER	hydrogen evolution reaction
Ir	iridium
MEA	membrane electrode assembly
MFC	mass flow control
MFM	mass flow meter
P	pressure
PTFE	polytetrafluoroethylene
SEI	solid electrolyte interphase
SEM	scanning electron microscopy
XRD	X-ray diffraction

1 (PDF)	DEFENSE TECHNICAL INFORMATION CTR DTIC OCA
1 (PDF)	DEVCOM ARL FCDD RLB CI TECH LIB